


## Article

# Environmental Analyses of Delayed-Feedback Control Effects in Continuum-Traffic Flow of Autonomous Vehicles

Ammar Jafaripournimchahi <sup>1</sup>, Yingfeng Cai <sup>1,\*</sup>, Hai Wang <sup>2</sup>  and Lu Sun <sup>3</sup><sup>1</sup> Automotive Engineering Research Institute, Jiangsu University, Zhenjiang 212013, China<sup>2</sup> School of Automotive and Traffic Engineering, Jiangsu University, Zhenjiang 212013, China<sup>3</sup> Department of Civil Engineering Technology, Environmental Management and Safety College of Engineering Technology, Rochester Institute of Technology, ENT-3102, New York, NY 14623, USA

\* Correspondence: caicaixiao0304@126.com

**Abstract:** Connected and Autonomous Vehicles are predicted to drive in a platoon with the aid of communication technologies to increase traffic flow efficiency while improving driving comfort, safety, fuel consumption, and exhaust emissions. However, some vehicles in a group may face communication failures. Such potential risks may even worsen the efficiency and safety of traffic flow and increase fuel consumption and exhaust emissions. Therefore, there is a need to propose an alternative scheme to control traffic flow effectively through vehicle-based information without the aid of communication technologies. In this paper, a deterministic acceleration model was developed considering the sensor's detection range to capture the underlying process of a car following the dynamics of autonomous vehicles. A delayed-feedback control was proposed based on the current and previous states of throttle angle to increase traffic flow stability and improve fuel consumption and exhaust emissions without the aid of communication technologies. Numerical simulations were carried out to study the impact of sensor detection range on micro-driving behavior and explore the effect of the proposed delayed-feedback control on the fuel consumption and exhaust emissions of autonomous vehicles in large-scale traffic flow. The numerical results certified that using delayed feedback with proper gains and delay time improved the total fuel consumption and exhaust emissions of autonomous vehicles.

**Keywords:** autonomous vehicles; inactive V2X communication environment; sensor detection range; car-following model; continuum-traffic flow; fuel consumption; exhaust emissions



**Citation:** Jafaripournimchahi, A.; Cai, Y.; Wang, H.; Sun, L. Environmental Analyses of Delayed-Feedback Control Effects in Continuum-Traffic Flow of Autonomous Vehicles. *Sustainability* **2022**, *14*, 11292. <https://doi.org/10.3390/su141811292>

Academic Editor: Xinqiang Chen

Received: 11 July 2022

Accepted: 6 September 2022

Published: 8 September 2022

**Publisher's Note:** MDPI stays neutral with regard to jurisdictional claims in published maps and institutional affiliations.



**Copyright:** © 2022 by the authors. Licensee MDPI, Basel, Switzerland. This article is an open access article distributed under the terms and conditions of the Creative Commons Attribution (CC BY) license (<https://creativecommons.org/licenses/by/4.0/>).

## 1. Introduction

The 26th United Nations Climate Change Conference (COP26) again brought the necessity of drastically reducing exhaust emissions to avoid climate catastrophe. The COVID-19 pandemic has also reminded us how much innovation is needed to prevent a climate disaster. To achieve the goal of reducing exhaust emissions, all economic sectors, policymakers, scientists, and nations need to mobilize their capability of decarbonization with a set of changes and actions. Among all economic sectors, the transportation sector accounts for a significant portion of exhaust emissions and alone contributes to approximately a quarter of the total fuel consumption and associated exhaust emissions in the world [1].

The United States Energy Information Administration (EIA) reported that, in 2021, motor vehicles consumed about 134.83 billion gallons of fuel in the transportation sector, which resulted in the emission of about 1018 MMmt of carbon dioxide (CO<sub>2</sub>). This amount was equal to about 82% of the total U.S. transportation sector CO<sub>2</sub> emissions and to about 30% of the total U.S. energy-related CO<sub>2</sub> emissions in 2021 [2]. As a result, the transportation sector must take an active role in addressing the challenge of climate change mitigation and assisting governments in meeting their exhaust emission reduction targets.

While the transportation sector continues to be the largest contributor to fuel consumption and exhaust emissions, a number of alternatives have been put forward to address the challenges of climate change mitigation. Using low-carbon fuels, innovating new vehicle technologies, identifying alternative power sources (e.g., hybrid and fuel cell vehicles), and operating vehicles more efficiently are all approaches to decreasing fuel consumption and exhaust emissions from transportation. However, traffic congestion, the most visible and pervasive transport problem, which is the main contributor to fuel consumption and exhaust emissions in the transportation sector, remains unsolved.

Over the last two decades, tremendous efforts have been made worldwide to address traffic congestion by adding lanes, widening roads, and implementing road pricing. However, the impacts of capacity-based congestion improvements are only piecemeal strategies that alone do not address the traffic congestion problem. Such a method of improvement only scratches the surface of the problem and eventually becomes marginal. Moreover, there may not always be enough land where there is a need to add lanes and widen roads. Recently, Information and Communication Technologies (ICT) embedded in autonomous vehicles have been developed dramatically in terms of hardware and software to create a reliable internet of vehicles, where individual vehicles can communicate with each other using vehicle-to-vehicle (V2V) technologies and infrastructure using Vehicle-to-Infrastructure (V2I) technologies, with the goal of increasing the safety and efficiency of traffic flow and decreasing fuel consumption and exhaust emissions [3–5].

Although such new technologies typically aim to increase the reliability and safety of autonomous vehicle operations, they also provide new opportunities for more active transportation systems to improve traffic flow stability, fuel consumption, and exhaust emissions. Among all these new technologies, V2V communication has been recognized as the most effective possible solution to traffic flow instability. The potential benefits that V2V communication can bring to traffic flow safety and stability, fuel consumption, and exhaust emissions have been evaluated by experiments and simulations [6–16].

However, the improvement of traffic flow stability with the aid of V2V communication technology is still negligible and plagued by several challenges, such as a lack of communication networks and cybersecurity threats. These potential risks may even worsen traffic flow stability and safety as well as increase fuel consumption and exhaust emissions [17–19].

Alternatively, another control strategy needs to be proposed that does not require communication between vehicles and relies only on each vehicle's information (i.e., current and previous). This strategy will maintain its longitudinal maneuvers consistent with the equilibrium state of traffic flow, reducing the fuel consumption and exhaust emissions caused by unstable traffic flow [20,21]. Such flexibility allows controllers to fully exploit the advantages of a vehicle's internal information to regulate its state. The delayed-feedback control strategy has proven to be one of the most convenient and effective strategies for controlling real chaotic systems without using any external information [22,23]. This control strategy was proposed based on the difference between the current state of the system and the previous one, in which the amplitude of the feedback signal was considered as a criterion of unstable periodic orbit stabilization. When the desired orbit is stabilized, the control signal will be eliminated [23].

Pyragas [23] proposed a delayed-feedback control to stabilize the unstable periodic orbits of a chaotic system. Considering this strategy, Just et al. [22] conducted numerical and experimental simulations on feedback control [23] and revealed that the success of the proposed control scheme depends on revolution around the unstable periodic orbit of the chaotic system.

Later, to alleviate traffic congestion, several researchers successfully implemented the delayed-feedback control to the controller design of car-following models. Konishi et al. [24] presented a decentralized delayed-feedback control for stabilizing the unstable behavior of a one-way coupled map model and found that incorporating the delayed-feedback control into car-following models results in the suppression of traffic congestion [25–27].

Zhao et al. [28], designed a new delayed-feedback control considering the velocity difference between the leading and following vehicles in a V2V environment and applied it to the optimal velocity (OV) model to suppress the traffic congestion induced by bottlenecks. Davis [29] developed delayed-feedback control using the velocity difference between a leading and a following vehicle as a feedback term and incorporated it into the FVD model to improve string stability. The impact of delayed-feedback control on traffic flow was investigated by Zhang et al. [30] through Hopf bifurcation analysis, and the results revealed that feedback control can postpone the occurrence of Hopf bifurcation and increase traffic flow stability effectively.

Considering both space headway and velocity differences as a feedback term, Jin et al. [31] developed a delayed-feedback control system to suppress traffic congestion in the OV model and demonstrated that the anti-interference capability of the OV model becomes stronger by using delayed-feedback control.

Furthermore, the recent advancement of vehicles' internal state sensors and internal communication technologies provide the opportunity for autonomous vehicles to measure the internal values of their dynamic systems (e.g., steering angle, throttle angle, brake torque) and transmit these data to the vehicle's control unit via the Controller Area Network (CAN) bus. This data, along with vehicle kinematic information (e.g., space headway, velocity, acceleration), can provide further understanding of a vehicle's current situation and its changing tendency, and result in improving traffic flow stability, fuel consumption, and exhaust emissions [32,33].

Several researchers have attempted to study the impact of throttle angle information on traffic flow and found that the transmission of throttle angle information between vehicles using V2V communication technologies increases the stability of traffic flow significantly [34–38]. However, there are four shortcomings in the previous research. (1) The existing research attempted to address the instability issue of traffic flow considering the leading vehicles' trajectory data through V2V communication technology, while this technology is still negligible and plagued by several challenges, and the harsh requirement that all vehicles must be equipped with dedicated short-range communication (DSRC) devices and constantly receive the accurate information of several vehicles ahead (possibly the entire traffic stream ahead) hinders the deployment of such technology (i.e., mixed traffic flow is composed of connected, autonomous, and human-driving vehicles). It can be noted that, when V2V communications are unavailable, autonomous vehicles exhibit similar driving behavior to Adaptive Cruise Control (ACC) vehicles that are already available on the market and have been proved to be string-unstable [19,39–41].

(2) The existing research captures the underlying process of acceleration decision-making of vehicles using the car-following models proposed for human driving vehicles. However, an autonomous vehicle has different car-following behavior considering its sensor detection range, which needs to be considered in modeling process. (3) They are either limited to specific scenarios or specific stability analyses at a microscopic level with limited numbers of vehicles and can hardly assess the effect of vehicles' topology on the stability of traffic flow due to scalability issues. (4) There is no specific study to explore the impact of autonomous vehicles on fuel consumption and exhaust emissions at a macroscopic level.

To fill the gaps, a deterministic acceleration model (i.e., Full Velocity Difference (FVD) model) that is used in the literature by the vast majority of studies [14,31,34,35,37,42–47] was developed in this paper considering the sensor detection range to model the car-following behavior of autonomous vehicles in an inactive V2I environment. Building upon the valuable contribution of delayed-feedback control, a solution was explored to reduce the fuel consumption and exhaust emissions of autonomous vehicles in an inactive V2I communication environment by taking advantage of the vehicle's throttle angle information at the current time and previous time. The feasible ranges of control parameters that ensure smooth traffic flow were derived from the perspective of the frequency domain via Hurwitz criteria and the  $H_\infty$  norm of transfer functions. Different from the previous models,

the developed model aimed to be robustly string-stable without requiring any external information from other unconnected vehicles.

Finally, numerical-based simulations were performed to study the impact of the sensor detection range on micro-driving behavior and explore the effect of delayed feedback control on the fuel consumption and exhaust emissions of autonomous vehicles in large-system traffic flow.

This paper is organized as follows: The Section 2 describes the procedures leading to the controlled car-following model and its stability analysis. The Section 3 proposes the continuum-traffic model based on the developed car-following model. In the Section 4, the numerical-based simulations are conducted, and the results are presented and discussed. The key findings and concluding remarks are provided in the last section.

## 2. Modeling Autonomous Vehicles in an Inactive V2I Environment

The acceleration decision-making of human-driving vehicles during car-following maneuvers has been extensively modeled using deterministic acceleration frameworks. Jiang et al. [48] proposed a deterministic acceleration model, called the full-velocity difference (FVD) model, as shown in Equation (1a), considering both negative and positive velocity differences between two consecutive vehicles to capture the underlying process of the acceleration decision making of human-driving vehicles during car-following maneuvers.

$$a_n(t) = a(V_n(y_n(t)) - v_n(t)) + \lambda \Delta v \quad (1a)$$

where  $a$  is the sensitivity coefficient of the driver,  $\lambda$  represents the weight coefficient of velocity difference,  $\Delta v_n(t)$  is the velocity difference between the following and leading vehicles, and  $V_n(y_n(t))$  is the optimal velocity proposed by Bando et al. [49] to calculate the optimal velocity of the human-driving vehicles at every decision point.

$$V_n(y_n(t)) = \frac{v_{\max}}{2} (\tanh(y_n(t) - y_{safe}) + \tanh(y_{safe})) \quad (1b)$$

where  $v_{\max}$  is the maximum velocity constraint from road signs (both VMS and conventional signs), and  $y_{safe}$  is the safe space headway, and  $y_n$  is the space headway between the following and leading vehicles. Considering the capability of autonomous vehicles to constantly monitor the surrounding vehicles via sensors (e.g., Lidar, Radar), an autonomous vehicle is certain about other vehicles' behavior and can react almost immediately to any changes in the leading vehicles (the reaction time of autonomous vehicles depends on the sensor's delay and other mechanical delays) [50,51]. Hence, a deterministic acceleration framework is suitable for modeling the car-following dynamics of autonomous vehicles [8].

In this study, the FVD model was developed considering sensor characteristics in the modeling process to capture the following dynamics of autonomous vehicles in the absence of communication. The developed model provides a greater realism than most deterministic acceleration models while capturing different congestion dynamics. It is worth mentioning that sensors are considered to produce the input data for the acceleration model.

In model (1a), the acceleration decision of an autonomous vehicle is affected by two terms: the difference between the optimal velocity, which depends on space headway and the current velocity, and the velocity difference between two successive vehicles. Since an autonomous vehicle cannot monitor a leading vehicle that is located outside of its sensors' detection range, it will be reasonable to presume that there is a stopped vehicle right outside of the sensors' detection range at the time of acceleration decision making [52]. Furthermore, if the leading vehicle is in the detection range of the autonomous vehicle's sensors, it will be reasonable to presume that the velocity of the autonomous vehicle needs to be low enough to allow the vehicle to stop when its leading vehicle decides to stop with its maximum deceleration rate [8].

Considering the above discussion, the maximum safe velocity ( $v_{\max}$ ) of the FVD model can be calculated at every decision point by using the following equation:

$$\begin{aligned} y_{safe} &= v_n \tau + \frac{v_{n+1}^2(t)}{2a_{n+1}^{\max,decc}} \\ y &= (x_{n+1} - x_n) + y_{safe} \\ y_n &= \min\{\text{sensor detection range}, y\} \\ v_{\max} &= \sqrt{(-2a_n^{\max,decc} y_n)} \end{aligned} \quad (2)$$

where  $a_n^{\max,decc}$  is the maximum deceleration of vehicle  $n$ ,  $a_{n+1}^{\max,decc}$  represents the maximum deceleration of vehicle  $n + 1$ ,  $x_n$  and  $x_{n+1}$  show the locations of vehicle,  $n$  and its leading vehicles respectively, and  $v_n \tau$  is the distance travelled during the reaction time.

Figure 1 depicts maximum safe velocity profile; any velocity is considered to be safe as long as it is below the maximum safe velocity.

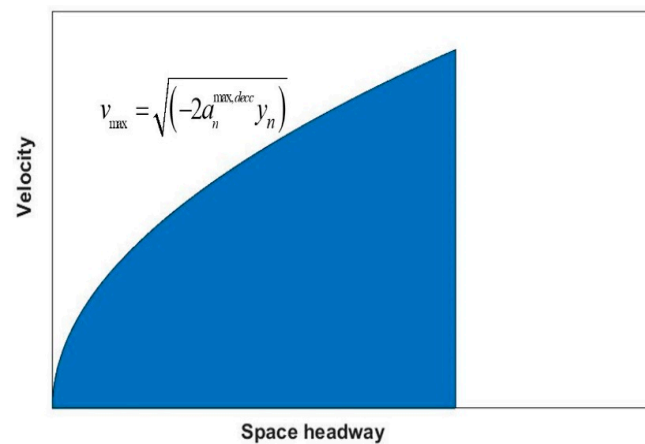


Figure 1. Maximum safe velocity profile [52].

Figure 2 shows the headway-equilibrium velocity curves under different values of sensor detection ranges. As we can see, under the same space headway variation, the equilibrium velocity decreases when the sensor detection range is reduced. From Figure 2, we can draw the conclusion that the stability of traffic flow becomes stronger when the sensor detection range is reduced, and such an improvement will be achieved at the expense of reducing the traffic flow velocity, which is undesirable in a real traffic environment.

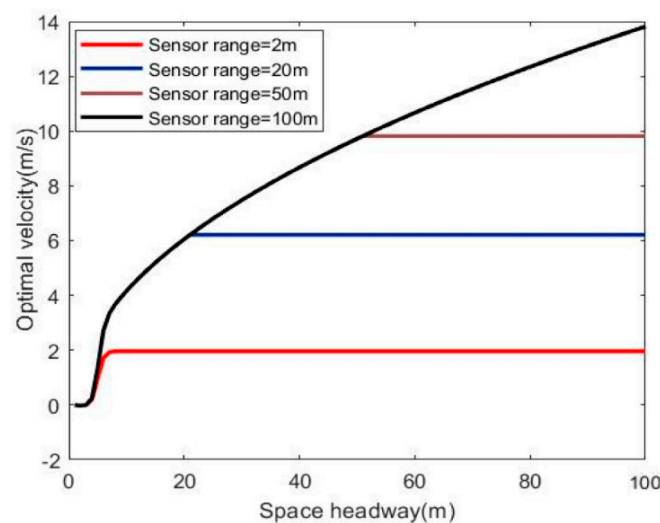


Figure 2. The headway-equilibrium velocity diagram for different sensor detection ranges.

When any external disturbances force traffic flow out of a steady state, the traffic flow remains stable if stability condition (3) is satisfied [48], otherwise any small traffic disturbance will gradually aggravate during the propagation process, eventually resulting in traffic congestion and increase fuel consumption and exhaust emissions.

$$V'_n(h) < \frac{a}{2} + \lambda \quad (3)$$

where  $h$  is the space headway between vehicles at steady-state traffic flow,  $a$  is the sensitivity coefficient of the driver, and  $\lambda$  is the weight coefficient of the velocity difference term in Equation (1a). In order to suppress traffic congestion when condition (3) is not satisfied, we designed a new delayed-feedback control based on throttle angle differences. The control signal is defined as follows:

$$u_i(t) = k(\theta_n(t) - \theta_n(t - \varepsilon)) \quad (4)$$

where  $k$  is the feedback gain of the throttle angle difference, which can be adjusted, and  $\varepsilon$  is the delay time of the throttle angle. The control signal  $u_i(t)$  is proportional to the electronic throttle angle difference of the considered AV vehicle at current time  $t$  and previous time  $(t - \varepsilon)$ . It should be noted that the control signal is activated only if traffic flow is unstable, otherwise it vanishes in stable traffic flow.

The control signal term is added to the developed model as follows:

$$\frac{dv_n(t)}{dt} = a(V(y_n(t)) - v_n(t)) + \lambda \Delta v_n(t) + u_i(t) \quad (5)$$

where  $\theta_n(t)$  and  $\theta_n(t - \delta)$  represent the throttle angle at current time  $t$  and previous time  $(t - \delta)$ , respectively. Since the electronic throttle angle directly affects both velocity and acceleration, the delayed-feedback control of throttle angle can be considered as an integration of the acceleration and velocity terms with time delay as follows [53]:

$$\theta_n(t) - \theta_n(t - \varepsilon) = \frac{1}{\omega} \left[ \frac{dv_n(t)}{dt} - \frac{dv_n(t - \varepsilon)}{dt} + \alpha(v_n(t) - v_n(t - \varepsilon)) \right] \quad (6)$$

where,  $\theta_0$  represents the steady state throttle angle for the corresponding steady state velocity  $v_\theta^0$ ,  $\omega$  and  $\alpha$  are parameters that change with  $v_\theta^0$  and need to be computed in advance at each type of engine operating point  $(\theta_0, v_\theta^0)$  and sorted in the look-up table for  $(\theta_0, v_\theta^0)$ , and  $d$  is unmodeled disturbances [53].

Putting Equation (6) into Equation (5), the equation of the controlled system becomes a neutral delay differential equation as follows:

$$\begin{aligned} \frac{dv_n(t)}{dt} &= a(V(y_n(t)) - v_n(t)) + \lambda \Delta v_n(t) + \frac{k}{\omega} \left[ \frac{dv_n(t)}{dt} - \frac{dv_n(t - \varepsilon)}{dt} + \alpha(v_n(t) - v_n(t - \varepsilon)) \right] \\ \frac{dy_n(t)}{dt} &= v_{n+1}(t) - v_n(t) \end{aligned} \quad (7)$$

To obtain the range of control gain  $k$ , we can conduct a stability analysis on a closed-loop traffic flow model with a delayed-feedback controller by using the traditional control theory. Zhang and Jarrett [54], noted that a slight deviation of the leading vehicle from steady state (e.g., a small variation in space headway or velocity) will force the following vehicle to react to this deviation. Then, we can add a slight deviation to Equation (7) as follows:

$$\begin{aligned} \frac{d\delta v_n(t)}{dt} &= a(\Lambda \delta y_n - \delta v_n(t)) + \lambda (\delta v_{n+1}(t) - \delta v_n(t)) + \frac{k}{\omega} \left[ \frac{d\delta v_n(t)}{dt} - \frac{d\delta v_n(t - \varepsilon)}{dt} + \alpha(\delta v_n(t) - \delta v_n(t - \varepsilon)) \right] \\ \frac{d\delta y_n(t)}{dt} &= \delta v_{n+1}(t) - \delta v_n(t) \end{aligned} \quad (8)$$

where  $\delta v_n(t) = v_n(t) - V(h)$ ,  $\delta v_n(t - \varepsilon) = v_n(t - \varepsilon) - V(h)$ ,  $\delta y_n(t) = y_n(t) - h$ , and  $\Lambda = \left. \frac{dV(y_n(t))}{dy_n(t)} \right|_{S_n(t)=h}$ .



Performing Laplace transform on Equation (8) as follows:

$$\begin{aligned} sV_n(s) &= a(\Lambda Y_n(s) - V_n(s)) + \lambda (V_{n+1}(s) - V_n(s)) + \frac{k}{\omega} [(1 - e^{-\varepsilon s})sV_n(s) + \alpha((1 - e^{-\varepsilon s})V_n(s))] \\ sY_n(s) &= V_{n+1}(s) - V_n(s) \end{aligned} \quad (9)$$

The matrix form of Equation (9) can be written as follows:

$$\begin{pmatrix} V_n(s) \\ Y_n(s) \end{pmatrix} = M \cdot \begin{pmatrix} \lambda \\ 1 \end{pmatrix} \frac{V_{n+1}(s)}{P(s)} \quad (10)$$

herein,  $Y_n(s) = L(\delta y_n(t))$ ,  $V_n(s) = L(\delta v_n(t))$  and  $L(\cdot)$  denotes the Laplace transform,  $M = \begin{bmatrix} s & a\Lambda \\ -1 & \omega s + \omega a + \omega \lambda + k(s + \alpha)(1 - e^{-\varepsilon s}) \end{bmatrix}$ , and  $P(s)$  represents the characteristics polynomial as:

$$D(s) = (\omega + k(1 - e^{-\varepsilon s}))s^2 + (\omega a + \omega \lambda + k\alpha(1 - e^{-\varepsilon s}))s + a\Lambda \quad (11)$$

Then, the transfer function can be described as follows:

$$G(s) = \frac{\lambda s + a\Lambda}{(\omega + k(1 - e^{-\varepsilon s}))s^2 + (\omega a + \omega \lambda + k\alpha(1 - e^{-\varepsilon s}))s + a\Lambda} \quad (12)$$

According to classical control theory [26], traffic flow is stable and traffic jams will be dissipated if two of the following conditions are satisfied:

- (I)  $D(s)$  is stable.
- (II)  $\|G(s)\|_\infty \leq 1$ .

For condition (I), the characteristic function  $D(s)$  can be described as:

$$D(s) = P(s) - Q(s)e^{-\varepsilon s} \quad (13)$$

where  $P(s) = (\omega + k)s^2 + (\omega a + \omega \lambda + k\alpha)s + a\Lambda$ ,  $Q(s) = (ks^2 + kas)e^{-\varepsilon s}$ .

When  $\varepsilon = 0$ , Equation (13) can be written:

$$s^2 + (a + \lambda)s + \frac{a\Lambda}{\omega} = 0 \quad (14)$$

The Routh–Hurwitz stability criterion shows that Equation (14) is asymptotically stable for the following condition:

$$(a + \lambda) > 0 \text{ and } \frac{\Lambda}{\omega} > 0 \quad (15)$$

To derive the stability condition of the characteristic function  $D(s)$ , we can define the critical function  $F(w)$  [55]:

$$\begin{aligned} F(w) &= [\operatorname{Re}P(iw)]^2 + [\operatorname{Im}P(iw)]^2 - [\operatorname{Re}Q(iw)]^2 - [\operatorname{Im}Q(iw)]^2 \\ &= (-(\omega + k)w^2 + a\Lambda)^2 + (\omega a + \omega \lambda + k\alpha)^2 w^2 - k^2 w^4 - k^2 \alpha^2 w^2 = w^4 + m_1 w^2 + m_2 \end{aligned} \quad (16)$$

where  $m_1 = \omega^2(a + \lambda)^2 + 2k\alpha\omega(a + \lambda) - 2(\omega + k)a\Lambda$ ,  $m_2 = a^2\Lambda^2$ .

The characteristic function  $D(s)$  is stable if its critical function ( $F(w)$ ) has no real roots [56,57], that is, when  $m_1$  and  $m_2$  hold the following conditions:

$$m_1 \geq 0, m_2 \geq 0 \text{ or } m_1 < 0, m_1 - 4m_2 < 0 \quad (17)$$

Substituting  $m_1$  and  $m_2$  into Equation (21), we have:

$$\frac{\omega^2(a+\lambda)^2}{2} - \omega a \Lambda \geq k(a\Lambda - \alpha\omega(a + \lambda)), \Lambda^2 \geq 0$$

or

$$\frac{\omega^2(a+\lambda)^2}{2} - \omega a \Lambda < k(a\Lambda - \alpha\omega(a + \lambda)), \left(\omega^2(a + \lambda)^2 + 2k\alpha\omega(a + \lambda) - 2(\omega + k)a\Lambda\right)^2 < 4a^2\Lambda^2 \quad (18)$$

As long as condition (18) is satisfied, the characteristics polynomial  $P(s)$  is stable. To ensure that the self-delayed feedback controller meets condition (II), the  $H_\infty$ -norm of  $G(s)$  needs to be 1 or less, i.e., [43,44]:

$$\|G(s)\|_\infty = |G(jw)| = \sqrt{|G(jw)G(-jw)|} \leq 1 \quad (19)$$

Therefore, the inequality  $|G(jw)| \leq 1$  is satisfied for any  $w \in [0, +\infty)$ , if the following condition holds:

$$\left[-(\omega + k(1 - \cos(\varepsilon w)))\omega^2 + a\Lambda + k\alpha w \sin(\varepsilon w)\right]^2 + \left[(\omega a + \omega\lambda + k\alpha(1 - \cos(\varepsilon w))\omega - k \sin(\varepsilon w)\omega^2)^2 - a^2\Lambda^2 - \lambda^2\omega^2\right] \geq 0 \quad (20)$$

Consequently, the traffic congestion can be effectively suppressed using the delayed-feedback controller when the condition Equations (18) and (20) are met.

**Theorem 1.** *Suppose that the stability condition of an FVD model without delayed-feedback control fails to maintain the stability conditions and traffic congestion occurs in the uncontrolled proposed model. Traffic congestion can be suppressed using a delayed-feedback controller if the control gain  $k$  of the throttle angle difference and delay time  $\varepsilon$  can yield conditions (18) and (20) simultaneously.*

### 3. Continuum-Traffic Flow Formulation

Road network capacity and mobility at the macroscopic level are directly influenced by driving behavior at the microscopic level [58]. In order to study the impact of the delayed-feedback controller on continuum-traffic flow, we can derive a continuum-traffic-flow model from the controlled FVD model presented by Equation (7). The discrete variables of a following autonomous vehicle  $n$  in relation to its leading vehicle  $n + 1$  need to be transformed into continuous variables through a simple Taylor expansion [59].

We can transform the microscopic variables of Equation (7) into macroscopic ones through a simple Taylor expansion as follows [60].

$$\begin{aligned} v_{n+1}(t) &\rightarrow v(x + S, t), & V(y_n(t)) &\rightarrow V_e(\rho(x, t)), \lambda \rightarrow 1/\tau, & a &\rightarrow 1/T, & V'(y_n(t)) &\rightarrow \bar{V}'(h) \\ v_n(t) &\rightarrow v(x, t), \\ v_n(t) - v_n(t - \varepsilon) &\rightarrow \varepsilon v_t, & \frac{dv_n(t)}{dt} - \frac{dv_n(t - \varepsilon)}{dt} &\rightarrow \varepsilon v v_{xt}, & \Delta v_n(t) &\rightarrow v_x S + \frac{1}{2} v_{xx} S^2 \\ v_n(t - \varepsilon) &\rightarrow v(x, t - \varepsilon), \end{aligned}$$

where  $T$  is the traffic flow relaxation time. Through the density  $\rho$  and mean space headway, the equilibrium velocity  $V_e(\rho(x, t))$  and  $\bar{V}(h)$  are defined, respectively, to satisfy  $V_e(\rho(x, t)) = \bar{V}(h)$  and  $\bar{V}'(h) = -\rho^2 V_e'(\rho(x, t))$ .

The coefficient  $c$  represents the backward propagation velocity of small disturbances relative to the moving traffic stream and captures the leading term in the vehicle's reaction to the space headway variation. The new continuum-traffic-flow model can be established as follows:

$$\begin{aligned} \frac{\partial \rho}{\partial t} + \frac{\partial(\rho v)}{\partial x} &= 0 \\ \frac{\partial v}{\partial t} + \left(v - \frac{c}{1 - \phi\alpha}\right) \frac{\partial v}{\partial x} &= \frac{1}{T(1 - \phi\alpha)} (V_e(\rho) - v) + \frac{\phi}{1 - \phi\alpha} v v_{xt} + \mu(\varphi) v_{xx} \\ \mu(\varphi) &= \frac{c^2 \tau}{2(1 - \phi\alpha)} \end{aligned} \quad (21)$$

where  $c = \frac{S}{\tau}$ ,  $\phi = \frac{k\varepsilon}{\omega}$ .

The first term on the right side of Equation (21) constrains the system to behave as the LWR model and depicts the tendency of traffic-flow velocity for approaching the equilibrium velocity. The second term on the right side of Equation (21) captures the



unexpected deceleration and acceleration of vehicles in the traffic flow, which has significant impacts on traffic movement, fuel consumption, and exhaust emissions. The viscosity term  $\mu(\rho)$  involving the second derivative term of velocity is seen on the right side of Equation (21). The viscosity term in macroscopic traffic models has been detailed in [61] based on the strong resemblance between the Navier–Stokes equations of compressible fluids in one space dimension and macroscopic traffic flow models.

Lu Sun et al. [61], noted that continuum-traffic flow can be treated as same as a continuum fluid from the perspective of kinematic wave theory considering some constraints, and the viscosity term arises from fluid dynamic resembling the tendency of the driving behavior in resisting unexpected velocity variations in leading vehicles at the microscopic level, and results in constant velocity fluctuation in the phase plane [61]. The viscosity term  $\mu(\rho)$  is proportional to the product of the propagation velocity of a small disturbance, propagation time, control gain of a self-stabilizing controller, traffic density, and sensitivity coefficients. The viscosity term  $\mu(\rho)$  describes bottle-neck behavior, stop-and-go waves, unexpected acceleration/deceleration, and non-local changes in traffic conditions.

The new controlled continuum-traffic model preserves the anisotropic property of traffic flow, overlooked in most continuum-traffic-flow models [61], and responds only to downstream traffic variation. In addition, incorporating a delayed-feedback controller into the FVD model leads to an additional term for capturing the impact of unexpected deceleration and acceleration of vehicles in traffic flow. The replacement of the velocity gradient term with the density gradient term allows our model to outperform other macroscopic models in overcoming negative velocities (i.e., wrong-way travel).

#### 4. Numerical Simulations and Discussion

In this section, numerical-based investigations were conducted to explore the impacts of the sensor detection range and delayed-feedback control on the fuel consumption and exhaust emissions under two different traffic situations, where Case I was the departure process of autonomous vehicles using different sensor detection ranges, and Case II was the evolution of a small perturbation in large scale traffic flow using delayed-feedback control.

##### 4.1. Case I

Emulating the same scenario used by Jiang et al. [48], we studied the impact of the sensor detection range on each vehicle's velocity, total fuel consumption, and exhaust emissions at different time steps.

Assuming eight autonomous vehicles (Figure 3) are stopped in a group during the red period of a traffic signal with an identical space headway of 7.4 m at time  $t < 0$ . At time  $t = 0$ , the traffic signal shifts from red to its green period, and the first leading vehicle of the group instantly starts up, and the other vehicles gradually move and follow their direct leading vehicle. We chose the second vehicle and the seventh vehicle in the group to explore how different sensor detection ranges can affect the velocity and acceleration of the following vehicles during the departure process.

Figure 4a–d depicts the second and seventh vehicles' velocities and accelerations during the departure process using different sensor detection ranges. Figure 4a,c shows that as the sensor detection range increased, the autonomous vehicle's equilibrium velocity increased, and the following vehicles' starting delay decreased.

From Figure 4a–d, we can see that the seventh vehicle, which was close to the leader of the group, quickly responded to traffic signal changes using a large sensor detection range (50 m), but second vehicle, which was located far from the leader of the group, accelerated after some delay. This delay increased when the sensor detection range decreased. Comparing Figure 4a and Figure 4c, it can be found that when sensors detected one or two leading vehicles, the delay time was almost negligible. In contrast, more leading vehicles caused more delay time due to the potential confusion of echoes from previous or subsequent pulses of the sensors and also the accuracy range of distance, which is usually limited to 1–4 m.

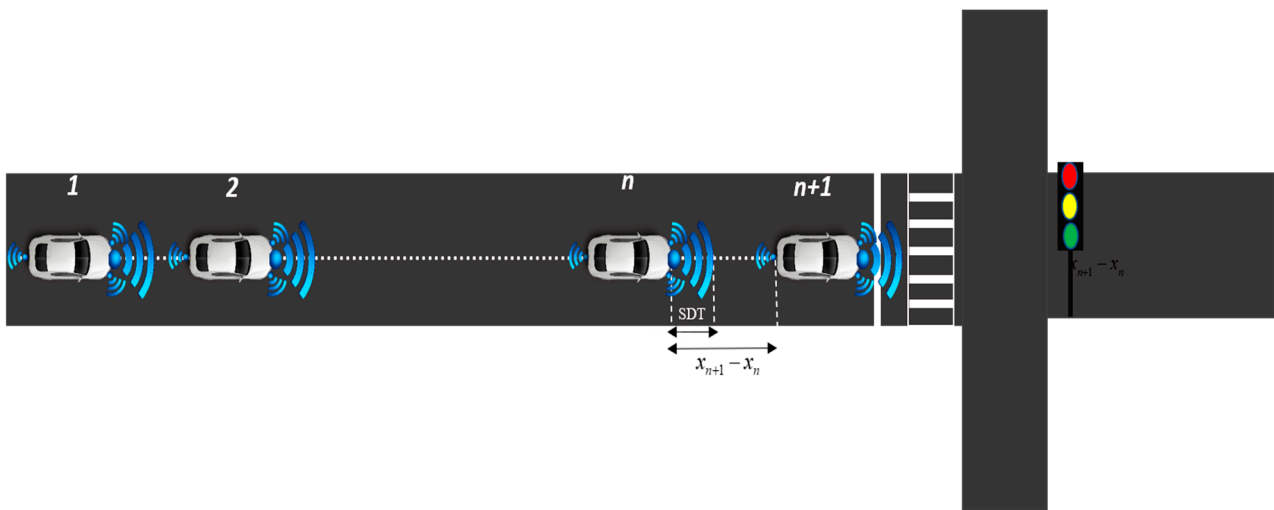
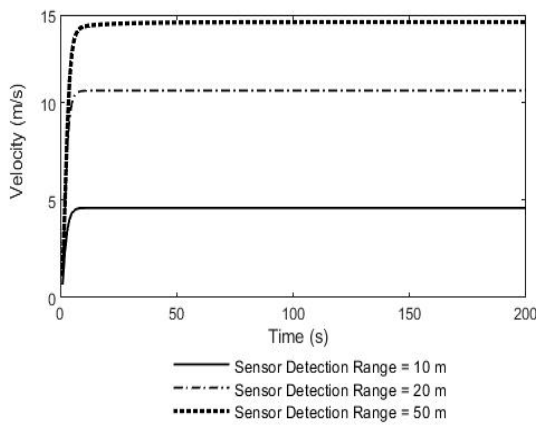
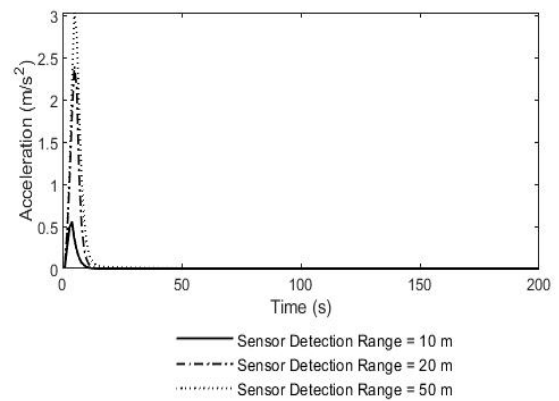


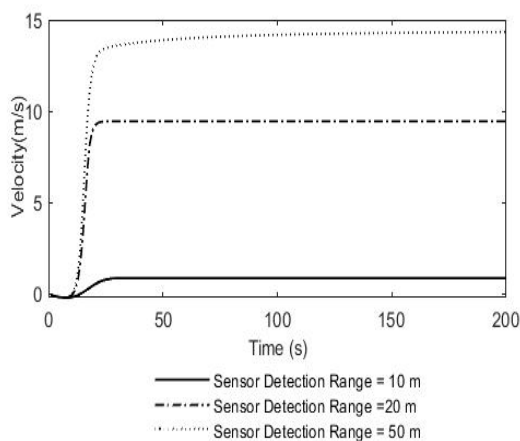
Figure 3. A group of eight autonomous vehicles proceed as the traffic light shifts from red to green.



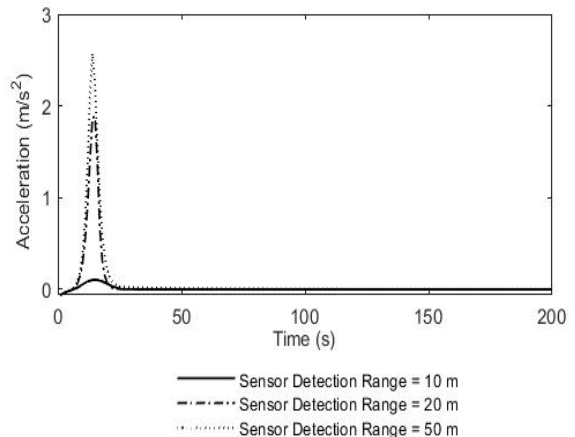
(a) Seventh vehicle's velocity



(b) Seventh vehicle's acceleration



(c) Second vehicle's velocity



(d) Second vehicle's acceleration

Figure 4. Vehicle's velocity and acceleration during the starting process with different sensor detection ranges; 10 m, 20 m, 50 m.

It is worth mentioning that autonomous vehicles use active and passive methods to measure the distance between leading vehicles [62]. The active methods measure the distance of leading vehicles on the principle of time-of-flight (ToF), in which the round-trip travel time of transmitted electromagnetic waves from a sensor to an object is measured,

while the passive methods do not emit electromagnetic waves and work on the basic principle of perceiving the light emitted from objects on a photosensitive surface through a lens to estimate the distance of the leading vehicle. In this paper, we assumed all vehicles were equipped with active sensors.

Figure 4b,d indicate that the acceleration process can be split into two phases. In the first phase, the vehicle using a large sensor detection range (50 m) applies the throttle pedal faster than the one using a short sensor detection range (10 m) and reaches a higher equilibrium velocity.

In the second phase, the vehicle using a short sensor detection range (10 m) releases the throttle pedal faster than the one using a large sensor detection range to reach the equilibrium velocity. The large sensor detection range not only increases the equilibrium velocity, but also benefits the following vehicles during the departure process because they can start applying the throttle pedal earlier to move forward faster when the traffic signal shifts to green and can avoid a higher level of acceleration and then release the throttle pedal a little to feel safe until they reach the equilibrium velocity. Furthermore, the results of Figure 4b,d show that the acceleration of autonomous vehicles simulated by our proposed model was within the limited range of empirical accelerations ( $0.4 \text{ m/s}^2$ ) observed by Helbing and Tilch [63]. From Figure 4a–d, we can draw the conclusion that the sensor detection range has prominent impact on autonomous vehicle micro-driving behavior during the departure process, which increases the equilibrium velocity of traffic flow and decreases delay time.

Next, we studied the impact of the sensor detection range on the vehicle's fuel consumption and exhaust emissions during the departure process using Tang's model [64] as follows:

$$\ln(MOE_e) = \sum_{i=0}^3 \sum_{j=0}^3 K_{i,j}^e \times v_i \times (v_t + vv_x)_j \quad (22)$$

where  $i$  and  $j$  are velocity power and acceleration power, respectively,  $MOE_e$  is the energy consumption rate (mL/s) or emission rate (mg/s),  $v_i$  is the instantaneous velocity,  $(v_t + vv_x)_j$  is the instantaneous acceleration, and  $k_{i,j}^e$  represent the coefficients of the regression model. The detailed values of the regression coefficients  $k_{i,j}^e$  can be found in Table 1 [64]. Tang's model computes the total fuel consumption and exhaust emissions based on the vehicle group trajectory data (i.e., position, velocity, and acceleration) of each road unit at each time step in the whole traffic flow.

**Table 1.** The regression coefficient [64].

	Fuel	CO	HC	NOx
$k_{0,0}^e$	−0.679439	0.887447	−0.728042	−1.067682
$k_{0,1}^e$	0.135273	0.148841	0.012211	0.254363
$k_{0,2}^e$	0.015946	0.030550	0.023371	0.008866
$k_{0,3}^e$	−0.001189	−0.001348	0.000093243	−0.000951
$k_{1,0}^e$	0.029665	0.070994	0.024950	0.046423
$k_{2,0}^e$	−0.000276	−0.000786	0.000205	0.000173
$k_{3,0}^e$	−0.000001487	0.000004616	0.000001949	0.000000569
$k_{1,1}^e$	0.004808	0.003870	0.010145	0.015482
$k_{1,2}^e$	−0.000020535	0.000093228	0.000103	−0.000131
$k_{1,3}^e$	$5.5409285 \times 10^{-8}$	0.000000706	0.000000618	0.000000328
$k_{2,1}^e$	0.000083329	−0.00926	0.000549	0.002876
$k_{2,2}^e$	0.000000937	0.000049181	0.000037592	0.00005866
$k_{2,3}^e$	$−2.479644 \times 10^{-8}$	−0.000000314	−0.000000213	0.00000024
$k_{3,1}^e$	−0.000061321	0.000046144	−0.000113	−0.000321
$k_{3,2}^e$	0.000000304	−0.000001410	0.000003310	0.000001943
$k_{3,3}^e$	$−4.467234 \times 10^{-9}$	$8.1724008 \times 10^{-9}$	$−1.739372 \times 10^{-8}$	$−1.257413 \times 10^{-8}$

Figure 5a–d illustrates the total fuel consumption and exhaust emissions of eight vehicles using different sensor detection ranges at  $t = 10$  s,  $t = 50$  s, and  $t = 200$  s, where the different colors of columns stand for different sensor detection ranges at given time steps. From Figure 5a, it can be obviously seen that when the sensor detection range at the time step of  $t = 10$  s increased, the total fuel consumption was enhanced since the vehicles needed more energy to speed up for the departure process. During the time steps ( $t = 50$  s,  $t = 200$  s), the total fuel consumption of the group of vehicles with a large detection range (50 m) gradually decreased through time, and the sensor detection range had little impact on the total fuel consumption as the vehicles at these time steps already reached their equilibrium velocity.

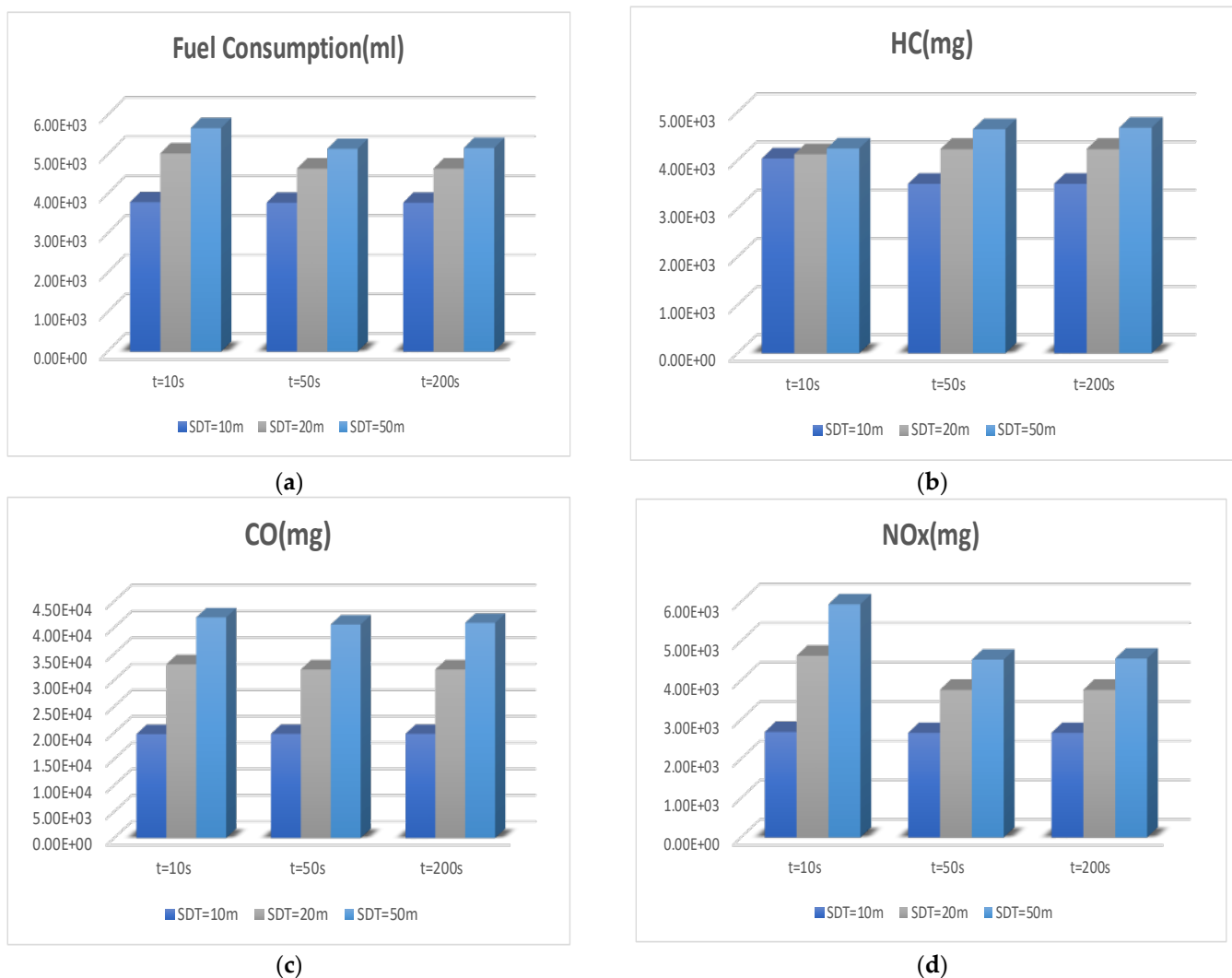


**Figure 5.** The total fuel consumption and exhaust emissions of eight vehicles at different time steps using different sensor detection ranges; (a) Fuel consumption, (b) HC, (c) CO, (d) NOx.

Considering Figures 4a,c and 5a, we can conclude that, however, the equilibrium velocity of autonomous vehicles significantly increased with the increase in the sensor detection range, but the total fuel consumption emissions decreased.

From Figure 5b–d, we have:

- (1) The sensor detection range had a lower impact on the total amount of HC than fuel consumption, and this impact increased over time. As the time increased, sensors with large detection ranges resulted in a bigger amount of HC,
- (2) The total amount of CO did not change at different time steps and increased when the sensor detection range was enhanced,

(3) At time step of  $t = 10$  s, when the sensor detection range increased, the total amount of NOx was enhanced, but this amount decreased significantly over time as the vehicles returned to the equilibrium velocity.

Consequently, the impact of the sensor detection range on the total amount of NOx and CO was more significant than the total amount of HC.

#### 4.2. Case II

The purpose of the numerical simulation conducted in this subsection was to evaluate the impact of the proposed delayed-feedback control of throttle angle difference on fuel consumption and exhaust emissions of autonomous vehicles in large scale traffic flow. We assumed that all autonomous vehicles were moving downstream in traffic with equilibrium velocity on a road with a length of  $L = 32.2$  km, were equipped with the same delayed-feedback controller and the same (Smart Micro) Automotive Radars (UMRR-00 Type 30) with a  $50 \text{ m} \pm 2.5\%$  detection range.

In the first scenario, the initial density of these vehicles was assumed to be  $\rho_0 = 0.055$  veh/m. A local small perturbation at  $t = 0$  on the distance ( $x = 10$  km) from the beginning of the road forced traffic flow out of its equilibrium state. The fuel consumption and exhaust emissions of the vehicles throughout the road, under different delayed times, and at time step  $t = 300$  s are depicted in Figure 6a–d. The fuel consumption and exhaust emissions were evaluated based on the vehicle trajectory data at each section of the road.

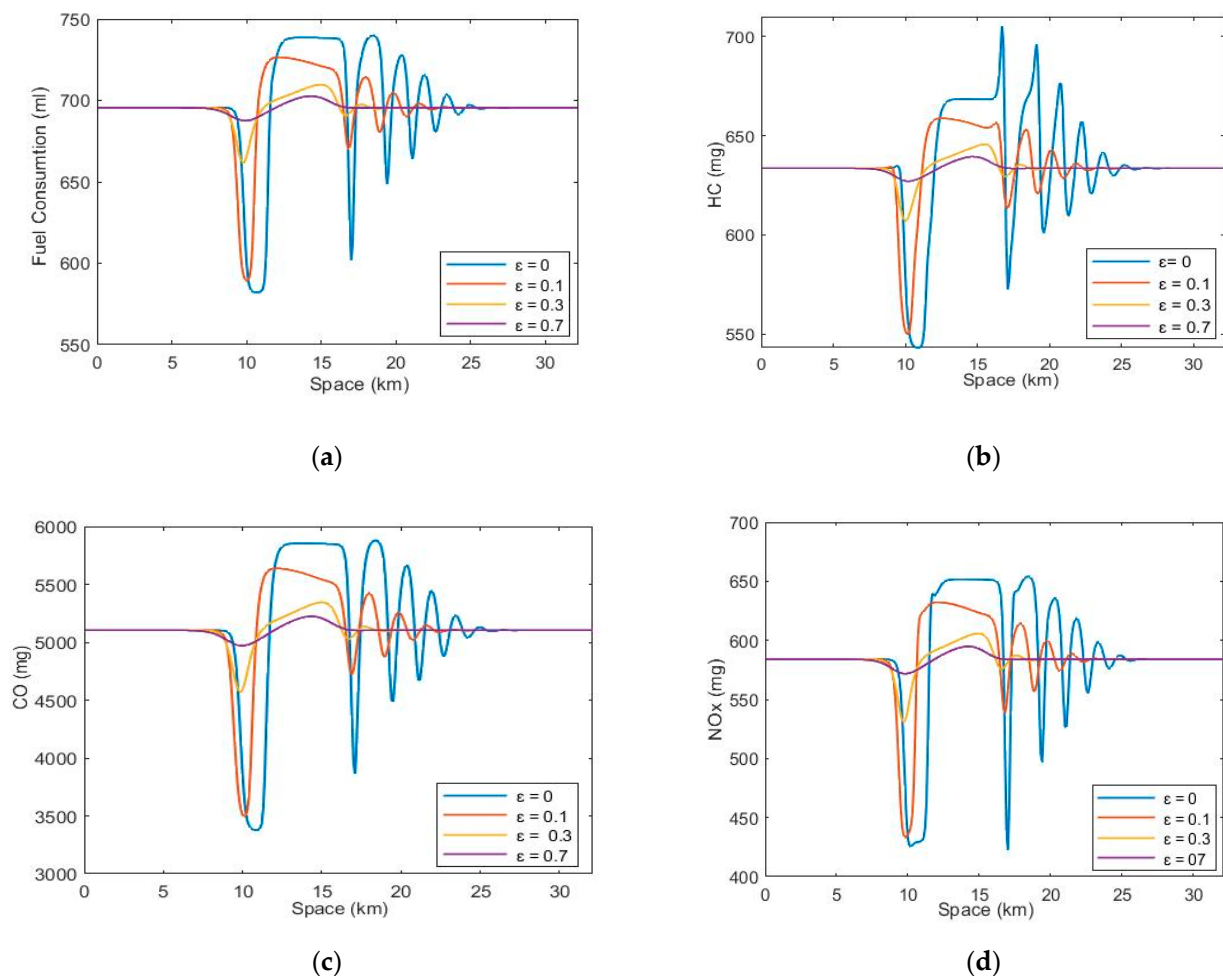


**Figure 6.** The fuel consumptions and exhaust emissions of the whole system at  $t = 300$  s under different values of  $\epsilon$  with initial density  $\rho_0 = 0.055$  veh/m,  $\tau = 0.3$  s,  $k = 0.1$ ,  $\alpha = 0.8 \text{ s}^{-1}$ ,  $\omega = 1.2 \text{ m/s}^{-2} \text{ degree}^{-1}$ : (a). Fuel consumption, (b). HC, (c). CO, (d). NOx.

From Figure 6a–d, we can see that the traffic flow was most unstable when the delayed feedback control of vehicles in traffic was inactive ( $\varepsilon = 0$ ), and evolved into uniform flow with the increase in delayed feedback time  $\varepsilon$ . It is obvious that the fuel consumption and exhaust emissions fluctuated the most when the delayed feedback control of the vehicles in traffic were inactive ( $\varepsilon = 0$ ) due to the frequent acceleration and deceleration in stop-go traffic. As shown in Figure 6a–d, the fuel consumption and exhaust emissions gradually reduced as the value of the delayed time  $\varepsilon$  was enhanced.

The fuel consumption and exhaust emissions of continuum-traffic flow with a higher initial density  $\rho_0 = 0.065$  veh/m at time step  $t = 300$  s and under different values of  $k$  are shown in Figure 7a–d as the second scenario of our simulation. From Figure 7a, it is obvious that when the delayed feedback control of vehicles was not activated, the fuel consumption was most unstable due to frequent velocity and acceleration changes during car-following maneuvers and was higher than when the delayed-feedback control was considered in the traffic flow. The effects of the delayed feedback control using the historical throttle angle information on the exhaust emissions presented in Figure 7b–d was the same as the impact of the delayed-feedback control on fuel consumption. It can be seen that when control gain  $k$  increased by a small number, the amplitude of exhaust emission fluctuations significantly decreased. When comparing Figure 6a–d with Figure 7a–d, we can see that when initial density was higher, the amplitude of fuel consumption and exhaust emission fluctuation increased when small perturbations occurred, and the controller was inactive. However, the trend of the horizontal curve in Figure 6 is almost the same as Figure 7. Consequently, choosing the proper delay time and feedback gain improved the traffic flow stability, suppressed traffic congestion, and also reduced fuel consumption and exhaust emissions.

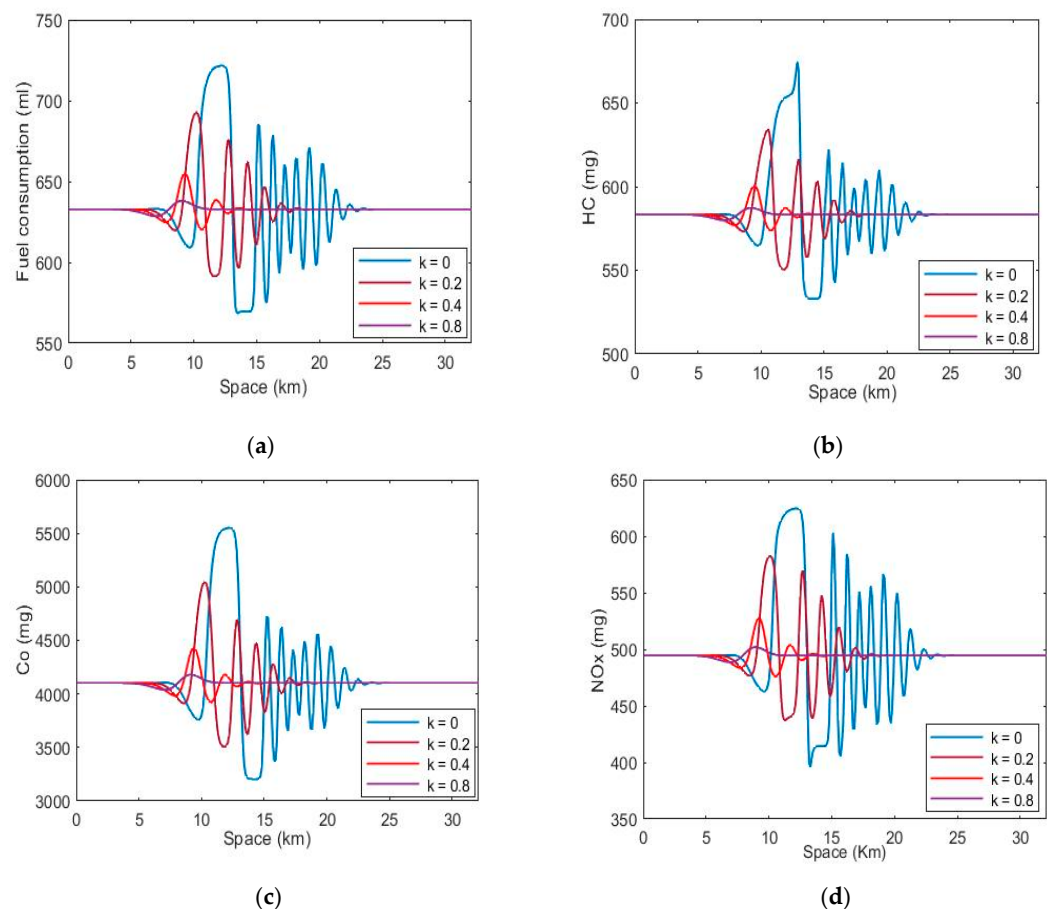


**Figure 7.** The total fuel consumptions and exhaust emissions in the process of traffic flow under different values of  $k$  with initial density  $\rho_0 = 0.065$  veh/m,  $\tau = 0.3$  s,  $\varepsilon = 0.1$ ,  $\alpha = 0.8$  s $^{-1}$ ,  $\omega = 1.2$  m/s $^{-2}$ degree $^{-1}$ ; (a). Fuel consumption, (b). HC, (c). CO, (d). NOx.



## 5. Conclusions

In this paper, a deterministic acceleration model was developed considering sensor detection range to capture the underlying process of the car-following dynamics of autonomous vehicles in an inactive V2I environment. The stability criterion of the developed car-following model was derived through the classical control method. The impact of the sensor detection range on the equilibrium velocity was investigated through numerical simulation. From the simulation results, we revealed that the equilibrium velocity of traffic flow reduced with the decrease in sensor detection range. The impact of the sensor detection range on the total fuel consumption and exhaust emissions during the departure process is being studied. The numerical simulations indicated that when the sensor detection range increased, the total fuel consumption and exhaust emissions at the beginning of the departure process increased, and then decreased over the time. Furthermore, when the stability condition of the deterministic acceleration model was not satisfied, we designed a delayed-feedback control using the difference between the current state of throttle angle and the previous state and integrated it with the developed deterministic acceleration model to improve traffic flow stability, fuel consumption, and exhaust emissions without the aid of communication. The impact of the designed delayed-feedback control on the fuel consumption and exhaust emissions of autonomous vehicles in large-scale traffic flow was studied through numerical-based investigations. The numerical results revealed that the fluctuating amplitude could be effectively alleviated when the designed delayed-feedback controller was applied with a proper delay time and feedback gain, and the traffic flow could quickly return to a steady state, which resulted in improving fuel consumption and exhaust emissions.

Without V2I communication, the autonomous vehicles' perception of the environment would be largely limited to their sensor detection range. The proposed controller utilized the throttle angle difference as the control input, which could directly control the engine without transcoding and editing the control signal. This could effectively decrease the response time of the control scheme, which is particularly suitable for roads without communication networks. The example presented in this study provided an insight into the impact of autonomous vehicles on fuel consumption and exhaust emissions. In addition, this paper studied the stability of macroscopic traffic flow on a single lane, while some important content, such as traffic flow safety and lane changing, were not considered.

In future work, we will investigate the impact of passive sensors, including mono-vision systems and stereo-vision systems on the car-following behavior of autonomous vehicles. Therefore, other research directions will study the impact of delayed feedback control on traffic flow safety and will consider more complex driving behaviors during the modeling process to depict real traffic environments.

**Author Contributions:** Conceptualization, A.J. and Y.C.; methodology, A.J.; software, A.J.; validation, A.J., Y.C. and H.W.; formal analysis, L.S.; investigation, A.J.; resources H.W.; data curation, Y.C.; writing—original draft preparation, A.J.; writing—review and editing, Y.C.; visualization, L.S.; supervision, Y.C.; project administration, L.S.; funding acquisition, Y.C. and H.W. All authors have read and agreed to the published version of the manuscript.

**Funding:** This study was sponsored in part by Key Research and Development Program of Jiangsu Province under grants BE2020083-3 and BE2019010-2, and the National Natural Science Foundation of China under grants 51050110143 and 51250110075, to which the authors are very grateful.

**Institutional Review Board Statement:** Not applicable.

**Informed Consent Statement:** Not applicable.

**Data Availability Statement:** The data published in this paper can be available and accessible from the corresponding author upon written official request with a legitimate justification.

**Acknowledgments:** This study was sponsored in part by Key Research and Development Program of Jiangsu Province under grants BE2020083-3 and BE2019010-2, and the National Natural Science Foundation of China under grants 51050110143 and 51250110075, to which the authors are very

grateful. The authors are also thankful to anonymous reviewers for their insightful comments and constructive suggestions, which helped us improve the content and presentation of the manuscript.

**Conflicts of Interest:** The authors declare no conflict of interest. The funders had no role in the design of the study; in the collection, analyses, or interpretation of data; in the writing of the manuscript; or in the decision to publish the results.

## References

1. Touratier-Muller, N.; Machat, K.; Jaussaud, J. Impact of French Governmental Policies to Reduce Freight Transportation CO<sub>2</sub> Emissions on Small- and Medium-Sized Companies. *J. Clean. Prod.* **2019**, *215*, 721–729. [[CrossRef](#)]
2. United States Energy Information Administration (EIA). Monthly Energy Review. 2022. Available online: <https://www.eia.gov/totalenergy/data/monthly/pdf/mer.pdf> (accessed on 1 August 2022).
3. González, D.; Pérez, J.; Milanés, V.; Nashashibi, F. A Review of Motion Planning Techniques for Automated Vehicles. *IEEE Trans. Intell. Transp. Syst.* **2016**, *17*, 1135–1145. [[CrossRef](#)]
4. Chen, Q.; Xu, L.; Zhou, Y.; Li, S. Finite Time Observer-based Super-twisting Sliding Mode Control for Vehicle Platoons with Guaranteed Strong String Stability. *IET Intell. Transp. Syst.* **2022**. [[CrossRef](#)]
5. Chen, Q.; Zhou, Y.; Ahn, S.; Xia, J.; Li, S.; Li, S. Robustly String Stable Longitudinal Control for Vehicle Platoons Under Communication Failures: A Generalized Extended State Observer-Based Control Approach. *IEEE Trans. Intell. Veh.* **2022**, *66*, 1. [[CrossRef](#)]
6. Liu, H.; Kan, X.; Shladover, S.E.; Lu, X.Y.; Ferlis, R.E. Modeling Impacts of Cooperative Adaptive Cruise Control on Mixed Traffic Flow in Multi-Lane Freeway Facilities. *Transp. Res. Part C Emerg. Technol.* **2018**, *95*, 261–279. [[CrossRef](#)]
7. Yao, Z.; Hu, R.; Wang, Y.; Jiang, Y.; Ran, B.; Chen, Y. Stability Analysis and the Fundamental Diagram for Mixed Connected Automated and Human-Driven Vehicles. *Phys. A Stat. Mech. Appl.* **2019**, *533*, 121931. [[CrossRef](#)]
8. Talebpour, A.; Mahmassani, H.S. Influence of Connected and Autonomous Vehicles on Traffic Flow Stability and Throughput. *Transp. Res. Part C Emerg. Technol.* **2016**, *71*, 143–163. [[CrossRef](#)]
9. Jafaripournimchahi, A.; Hu, W.; Sun, L. Nonlinear Stability Analysis for an Anticipation-Memory Car Following Model in the Era of Autonomous and Connected Vehicles. In Proceedings of the 2020 International Conference on Urban Engineering and Management Science, ICUEMS 2020, Zhuhai, China, 24–26 April 2020. [[CrossRef](#)]
10. Naus, G.J.L.; Vugts, R.P.A.; Ploeg, J.; van de Molengraft, M.J.G.; Steinbuch, M. String-Stable CACC Design and Experimental Validation: A Frequency-Domain Approach. *IEEE Trans. Veh. Technol.* **2010**, *59*, 4268–4279. [[CrossRef](#)]
11. Van Arem, B.; Tampere, C.M.J.; Malone, K.M. Modelling Traffic Flows with Intelligent Cars and Intelligent Roads. In Proceedings of the IEEE IV2003 Intelligent Vehicles Symposium, Proceedings (Cat. No. 03TH8683), Columbus, OH, USA, 9–11 June 2003; pp. 456–461.
12. Jing, J.; Kurt, A.; Ozatay, E.; Michelini, J.; Filev, D.; Ozguner, U. Vehicle Speed Prediction in a Convoy Using V2V Communication. In Proceedings of the 2015 IEEE 18th International Conference on Intelligent Transportation Systems, Gran Canaria, Spain, 15–18 September 2015; pp. 2861–2868.
13. Shladover, S.E.; Su, D.; Lu, X.-Y. Impacts of Cooperative Adaptive Cruise Control on Freeway Traffic Flow. *Transp. Res. Rec.* **2012**, *2324*, 63–70. [[CrossRef](#)]
14. Jafaripournimchahi, A.; Hu, W.; Sun, L. An Asymmetric-Anticipation Car-Following Model in the Era of Autonomous-Connected and Human-Driving Vehicles. *J. Adv. Transp.* **2020**, *2020*, 8865814. [[CrossRef](#)]
15. Vahidi, A.; Sciarretta, A. Energy Saving Potentials of Connected and Automated Vehicles. *Transp. Res. Part C Emerg. Technol.* **2018**, *95*, 822–843. [[CrossRef](#)]
16. Brown, K.E.; Dodder, R. Energy and Emissions Implications of Automated Vehicles in the U.S. Energy System. *Transp. Res. Part D Transp. Environ.* **2019**, *77*, 132–147. [[CrossRef](#)] [[PubMed](#)]
17. Milanés, V.; Shladover, S.E.; Spring, J.; Nowakowski, C.; Kawazoe, H.; Nakamura, M. Cooperative adaptive cruise control in real traffic situations. *IEEE Trans. Intell. Transp. Syst.* **2014**, *15*, 296–305. [[CrossRef](#)]
18. Sun, L.; Jafaripournimchahi, A.; Hu, W. A Forward-Looking Anticipative Viscous High-Order Continuum Model Considering Two Leading Vehicles for Traffic Flow through Wireless V2X Communication in Autonomous and Connected Vehicle Environment. *Phys. A Stat. Mech. Its Appl.* **2020**, *556*, 124589. [[CrossRef](#)]
19. Milanés, V.; Shladover, S.E. Modeling Cooperative and Autonomous Adaptive Cruise Control Dynamic Responses Using Experimental Data. *Transp. Res. Part C Emerg. Technol.* **2014**, *48*, 285–300. [[CrossRef](#)]
20. Qiu, H.J.F.; Ho, I.W.-H.; Chi, K.T.; Xie, Y. A Methodology for Studying 802.11 p VANET Broadcasting Performance with Practical Vehicle Distribution. *IEEE Trans. Veh. Technol.* **2014**, *64*, 4756–4769. [[CrossRef](#)]
21. Jafaripournimchahi, A.; Cai, Y.; Wang, H.; Sun, L.; Yang, B. Stability Analysis of Delayed-Feedback Control Effect in the Continuum Traffic Flow of Autonomous Vehicles without V2I Communication. *Phys. A Stat. Mech. Appl.* **2022**, *605*, 127975. [[CrossRef](#)]
22. Just, W.; Bernard, T.; Ostheimer, M.; Reibold, E.; Benner, H. Mechanism of Time-Delayed Feedback Control. *Phys. Rev. Lett.* **1997**, *78*, 203. [[CrossRef](#)]
23. Pyragas, K. Continuous Control of Chaos by Self-Controlling Feedback. *Phys. Lett. A* **1992**, *170*, 421–428. [[CrossRef](#)]

24. Konishi, K.; Hirai, M.; Kokame, H. Decentralized Delayed-Feedback Control of a Coupled Map Model for Open Flow. *Phys. Rev. E* **1998**, *58*, 3055. [[CrossRef](#)]
25. Konishi, K.; Kokame, H.; Hirata, K. Delayed-Feedback Control of an Optimal Velocity Traffic Model. In Proceedings of the 2000 2nd International Conference. Control of Oscillations and Chaos. Proceedings (Cat. No. 00TH8521), St. Petersburg, Russia, 5–7 July 2000; Volume 2, pp. 221–224.
26. Konishi, K.; Kokame, H.; Hirata, K. Decentralized Delayed-Feedback Control of an Optimal Velocity Traffic Model. *Eur. Phys. J. B-Condens. Matter Complex Syst.* **2000**, *15*, 715–722. [[CrossRef](#)]
27. Konishi, K.; Kokame, H.; Hirata, K. Coupled Map Car-Following Model and Its Delayed-Feedback Control. *Phys. Rev. E* **1999**, *60*, 4000. [[CrossRef](#)] [[PubMed](#)]
28. Zhao, X.; Gao, Z. Controlling Traffic Jams by a Feedback Signal. *Eur. Phys. J. B-Condens. Matter Complex Syst.* **2005**, *43*, 565–572. [[CrossRef](#)]
29. Davis, L.C. Stability of Adaptive Cruise Control Systems Taking Account of Vehicle Response Time and Delay. *Phys. Lett. A* **2012**, *376*, 2658–2662. [[CrossRef](#)]
30. Zhang, Y.; Xue, Y.; Zhang, P.; Fan, D.; di He, H. Bifurcation Analysis of Traffic Flow through an Improved Car-Following Model Considering the Time-Delayed Velocity Difference. *Phys. A Stat. Mech. Appl.* **2019**, *514*, 133–140. [[CrossRef](#)]
31. Jin, Y.; Hu, H. Stabilization of Traffic Flow in Optimal Velocity Model via Delayed-Feedback Control. *Commun. Nonlinear Sci. Numer. Simul.* **2013**, *18*, 1027–1034. [[CrossRef](#)]
32. Cai, Y.; Luan, T.; Gao, H.; Wang, H.; Chen, L.; Li, Y.; Sotelo, M.A.; Li, Z. YOLOv4-5D: An Effective and Efficient Object Detector for Autonomous Driving. *IEEE Trans. Instrum. Meas.* **2021**, *70*, 4503613. [[CrossRef](#)]
33. Wang, H.; Chen, Y.; Cai, Y.; Chen, L.; Li, Y.; Sotelo, M.A.; Li, Z. SFNet-N: An Improved SFNet Algorithm for Semantic Segmentation of Low-Light Autonomous Driving Road Scenes. *IEEE Trans. Intell. Transp. Syst.* **2022**, 1–13. [[CrossRef](#)]
34. Li, Y.; Zhang, L.; Peeta, S.; He, X.; Zheng, T.; Li, Y. A Car-Following Model Considering the Effect of Electronic Throttle Opening Angle under Connected Environment. *Nonlinear Dyn.* **2016**, *85*, 2115–2125. [[CrossRef](#)]
35. Chen, L.; Zhang, Y.; Li, K.; Li, Q.; Zheng, Q. Car-Following Model of Connected and Autonomous Vehicles Considering Both Average Headway and Electronic Throttle Angle. *Mod. Phys. Lett. B* **2021**, *35*, 2150257. [[CrossRef](#)]
36. Qin, Y.; Wang, H. Analytical Framework of String Stability of Connected and Autonomous Platoons with Electronic Throttle Angle Feedback. *Transp. A Transp. Sci.* **2021**, *17*, 59–80. [[CrossRef](#)]
37. Li, S.; Cheng, R.; Ge, H. An Improved Car-Following Model Considering Electronic Throttle Dynamics and Delayed Velocity Difference. *Phys. A Stat. Mech. Appl.* **2020**, *558*, 125015. [[CrossRef](#)]
38. Li, Y.; Zhao, H.; Zheng, T.; Sun, F.; Feng, H. Non-Lane-Discipline-Based Car-Following Model Incorporating the Electronic Throttle Dynamics under Connected Environment. *Nonlinear Dyn.* **2017**, *90*, 2345–2358. [[CrossRef](#)]
39. Gunter, G.; Gloudemans, D.; Stern, R.E.; McQuade, S.; Bhadani, R.; Bunting, M.; Delle Monache, M.L.; Lysecky, R.; Seibold, B.; Sprinkle, J. Are Commercially Implemented Adaptive Cruise Control Systems String Stable? *IEEE Trans. Intell. Transp. Syst.* **2020**, *22*, 6992–7003. [[CrossRef](#)]
40. Sugiyama, Y.; Fukui, M.; Kikuchi, M.; Hasebe, K.; Nakayama, A.; Nishinari, K.; Tadaki, S.; Yukawa, S. Traffic Jams without Bottlenecks—Experimental Evidence for the Physical Mechanism of the Formation of a Jam. *New J. Phys.* **2008**, *10*, 033001. [[CrossRef](#)]
41. Sun, Y.; Olaru, D.; Smith, B.; Greaves, S.; Collins, A. Road to Autonomous Vehicles in Australia: A Comparative Literature Review. In Proceedings of the Australasian Transport Research Forum, Melbourne, Australia, 16–18 November 2016; pp. 16–18.
42. An, S.; Xu, L.; Qian, L.; Chen, G.; Luo, H.; Li, F. Car-Following Model for Autonomous Vehicles and Mixed Traffic Flow Analysis Based on Discrete Following Interval. *Phys. A Stat. Mech. Appl.* **2020**, *560*, 125246. [[CrossRef](#)]
43. Peng, G.; Yang, S.; Xia, D.; Li, X. Delayed-Feedback Control in a Car-Following Model with the Combination of V2V Communication. *Phys. A Stat. Mech. Appl.* **2019**, *526*, 120912. [[CrossRef](#)]
44. Wang, T.; Zhang, Y.; Zhang, J.; Li, Z.; Li, S. New Feedback Control Strategy for Optimal Velocity Traffic Model. *Phys. A Stat. Mech. Appl.* **2020**, *559*, 125053. [[CrossRef](#)]
45. Li, Y.; Sun, D.; Liu, W. Feedback Control of Traffic Jam Based on the Full Velocity Difference Car-Following Model. *J. Inf. Comput. Sci.* **2012**, *9*, 719–730.
46. Jafaripournimchahi, A.; Sun, L.; Hu, W. Driver’s Anticipation and Memory Driving Car-Following Model. *J. Adv. Transp.* **2020**, *2020*, 4343658. [[CrossRef](#)]
47. Jafaripournimchahi, A.; Cai, Y.; Wang, H.; Sun, L.; Weng, J. Integrated-Hybrid Framework for Connected and Autonomous Vehicles Microscopic Traffic Flow Modelling. *J. Adv. Transp.* **2022**, *2022*, 2253697. [[CrossRef](#)]
48. Jiang, R.; Wu, Q.; Zhu, Z. Full Velocity Difference Model for a Car-Following Theory. *Phys. Rev. E* **2001**, *64*, 017101. [[CrossRef](#)]
49. Bando, M.; Hasebe, K.; Nakayama, A.; Shibata, A.; Sugiyama, Y. Dynamical Model of Traffic Congestion and Numerical Simulation. *Phys. Rev. E* **1995**, *51*, 1035. [[CrossRef](#)] [[PubMed](#)]
50. Chen, X.; Wu, S.; Shi, C.; Huang, Y.; Yang, Y.; Ke, R.; Zhao, J. Sensing Data Supported Traffic Flow Prediction via Denoising Schemes and ANN: A Comparison. *IEEE Sens. J.* **2020**, *20*, 14317–14328. [[CrossRef](#)]
51. Chen, X.; Ling, J.; Wang, S.; Yang, Y.; Luo, L.; Yan, Y. Ship Detection from Coastal Surveillance Videos via an Ensemble Canny-Gaussian-Morphology Framework. *J. Navig.* **2021**, *74*, 1252–1266. [[CrossRef](#)]

52. Reece, D.A.; Shafer, S.A. A Computational Model of Driving for Autonomous Vehicles. *Transp. Res. Part A Policy Pract.* **1993**, *27*, 23–50. [[CrossRef](#)]
53. Ioannou, P.; Xu, Z. Throttle and Brake Control Systems for Automatic Vehicle Following. *IVHS J.* **1994**, *1*, 345–377. [[CrossRef](#)]
54. Zhang, X.; Jarrett, D.F. Stability Analysis of the Classical Car-Following Model. *Transp. Res. Part B Methodol.* **1997**, *31*, 441–462. [[CrossRef](#)]
55. Chowdhury, D.; Santen, L.; Schadschneider, A. Statistical Physics of Vehicular Traffic and Some Related Systems. *Phys. Rep.* **2000**, *329*, 199–329. [[CrossRef](#)]
56. Hu, H.Y.; Wang, Z.H. *Dynamics of Controlled Mechanical Systems with Delayed Feedback*; Springer Science & Business Media: Berlin/Heidelberg, Germany, 2002; ISBN 3540437339.
57. Hu, H.Y.; Wang, Z.H. Stability Analysis of Damped SDOF Systems with Two Time Delays in State Feedback. *J. Sound Vib.* **1998**, *214*, 213–225. [[CrossRef](#)]
58. Whitham, G.B. *Linear and Nonlinear Waves*; John Wiley & Sons Inc.: New York, NY, USA, 1974.
59. Zhai, C.; Wu, W. A Continuum Model with Traffic Interruption Probability and Electronic Throttle Opening Angle Effect under Connected Vehicle Environment. *Eur. Phys. J. B* **2020**, *93*, 52. [[CrossRef](#)]
60. Jiang, R.; Wu, Q.-S.; Zhu, Z.-J. A New Continuum Model for Traffic Flow and Numerical Tests. *Transp. Res. Part B Methodol.* **2002**, *36*, 405–419. [[CrossRef](#)]
61. Sun, L.; Jafaripournimchahi, A.; Kornhauser, A.; Hu, W. A New Higher-Order Viscous Continuum Traffic Flow Model Considering Driver Memory in the Era of Autonomous and Connected Vehicles. *Phys. A Stat. Mech. Appl.* **2020**, *547*, 123829. [[CrossRef](#)]
62. van Brummelen, J.; O'Brien, M.; Gruyer, D.; Najjaran, H. Autonomous Vehicle Perception: The Technology of Today and Tomorrow. *Transp. Res. Part C Emerg. Technol.* **2018**, *89*, 384–406. [[CrossRef](#)]
63. Helbing, D.; Tilch, B. Generalized Force Model of Traffic Dynamics. *Phys. Rev. E* **1998**, *58*, 133–138. [[CrossRef](#)]
64. Tang, T.-Q.; Huang, H.-J.; Shang, H.-Y. An Extended Macro Traffic Flow Model Accounting for the Driver's Bounded Rationality and Numerical Tests. *Phys. A Stat. Mech. Appl.* **2017**, *468*, 322–333. [[CrossRef](#)]